Surface Morphology of Nafion at Hydrated and Dehydrated Conditions

ARTICLE *in* MACROMOLECULES · MARCH 2013

Impact Factor: 5.8 · DOI: 10.1021/ma302399e

Macromolecules

Article

pubs.acs.org/Macromolecules

Surface Morphology of Nafion at Hydrated and Dehydrated Conditions

James R. O'Dea,† Nicholas J. Economou, and Steven K. Buratto*

Department of Chemistry and Biochemistry, University of California, Santa Barbara, California 93106-9510, United States

Supporting Information

ABSTRACT: The relation between proton exchange membrane (PEM) hydration and fuel cell performance has been well documented at the macroscopic scale. Understanding how changes in membrane water content affect the organization of proton conducting domains at the micrometer and submicrometer scales is a sought-after goal in the rational design of higher performing PEMs. Using atomic force microscopy phase and current imaging, we have resolved proton conducting domains at the surface of Nafion membranes at dehydrated, ambient, and hydrated conditions, observing a unique morphology at each membrane water content. At ambient conditions, Nafion's surface morphology resembles that proposed in the parallel-pore and bicontinuous network models, with the exception that hydrophilic domains are larger at the surface of Nafion compared to the bulk. At hydrated conditions, a network of wormlike, insulating domains extends several micrometers over Nafion's surface with more conductive, water-rich regions found between these fibrillar features. Neither the surface morphology observed at ambient conditions nor at hydrated conditions persists in dehydrated membranes, which instead exhibit a low coverage of isolated hydrophilic surface domains that, remarkably, are similar in size to such domains at ambient conditions. These observations affirm properties distinct to Nafion's surface and provide morphological evidence for the low conductivity observed in Nafion at dehydrated conditions and the high conductivity observed at hydrated conditions.

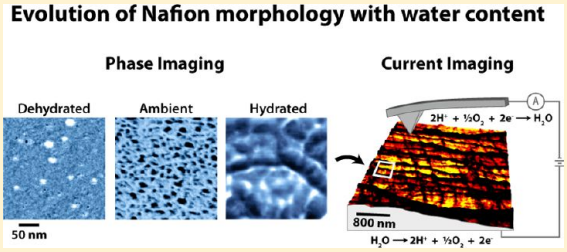

INTRODUCTION

Proton exchange membrane (PEM) fuel cell performance depends on the electrolyte's ability to transport protons from the anode to the cathode. In all but anhydrous PEMs,[1−4] proton transport in polymer electrolytes is critically linked to membrane hydration.[5−9] This dependence has been described on the molecular scale in perfluorosulfonic acid PEMs such as DuPont's Nafion membrane wherein proton conduction occurs along hydrated sulfonic acid groups through a combination of (1) structural diffusion[10] in which protons are passed along a chain of water molecules via the cleavage and formation of hydrogen bonds and (2) vehicular diffusion[11] in which individual water molecules shuttle protons as hydrated ions.[7−9] In the pursuit of higher performing PEMs, it has been shown that the morphology of ion conducting domains (i.e., their size, occurrence, and connectivity) also greatly affects proton transport.[12−15] For example, in membranes with the same chemical composition yet different copolymer architectures, Tsang et al. showed that a cluster morphology of ion domains in graft copolymers increased proton concentration and conductivity at high water contents compared to a lamellar morphology in diblock copolymers.[16]

Because fuel cell performance is related to both the hydration and morphology of proton conducting domains, the goal of this work is to explore the interplay between membrane water content and the arrangement of proton conducting domains, in particular at the membrane's surface as it forms a critical interface with the electrode and catalyst layer.[17] Specifically, we examine the surface morphology of Nafion membranes using atomic force microscopy (AFM) phase and current imaging. In the former, phase shifts (i.e., temporal lags or leads) between an oscillating cantilever and the ac signal used to drive it are related to the power dissipated by tip−sample interactions,[18,19] which enables mapping of the hydrophilic and hydrophobic domains at the surface of a PEM.[20−22] Current imaging is used in this work to assign morphologies when contrast in phase images is dominated by topography and changes in topography rather than chemical composition.

Previous studies of Nafion's morphology as a function of membrane hydration have primarily relied on bulk-averaged measurements from small- and wide-angle X-ray and neutron scattering.[23−27] These techniques have greatly contributed to the understanding of Nafion, yet morphological descriptions of aperiodic materials such as Nafion are limited by interpretation of a single scattering peak, despite insights gained from power law dependencies of scattering curves. Excluding maximum entropy reconstructions,[28] conclusions drawn from scattering studies involve *a priori* assumptions regarding the distribution and shape of scattering objects. Morphologies proposed from scattering measurements of Nafion include polymer rods or

Received: November 20, 2012
Revised: February 6, 2013
Published: March 15, 2013

   dx.doi.org/10.1021/ma302399e | *Macromolecules* 2013, 46, 2267−2274

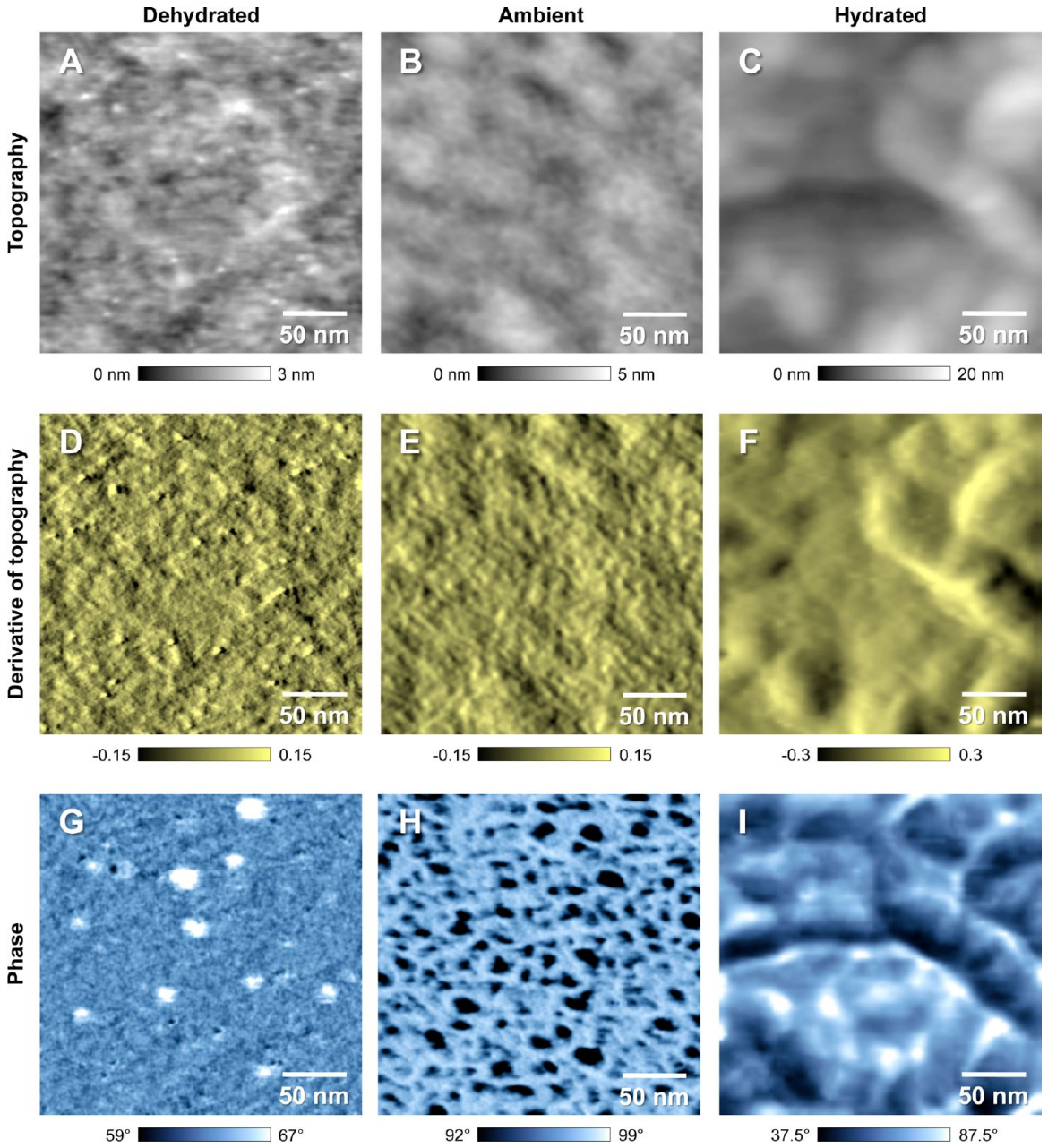

Figure 1. (A–C) Topography, (D–F) derivative of topography, and (G–I) phase images (250 nm × 250 nm) of Nafion 212 membranes at dehydrated (3% RH), ambient (49% RH), and hydrated (95% RH) conditions. As described in the text, phase images reflect the distribution of hydrophilic and hydrophobic surface domains. No measurable difference in morphology was observed over the range of ambient relative humidities that existed in our laboratory (30%–75% RH).

ribbons surrounded by ionic groups (micelle)[23,24] and, conversely, ionic groups surrounded by the polymer backbone (inverted micelle).[27] While these models represent seemingly disparate structures, some of their differences arise from consideration of membranes with different water contents.[29,30] While the parallel pore model is well supported by scattering data, this model is limited to descriptions of Nafion's morphology on length scales less than 20 nm,[27] whereas proton conduction occurs over tens of micrometers in PEMs. This underlies the importance of studying PEM morphology on more than one length scale, which is accessible with the phase and current imaging experiments reported here. Specifically, atomic force microscopy allows the properties of a material to be probed at lengths less than 10 nm to greater than 10 μm.

Previous work using AFM to describe the surface morphology of Nafion as a function of membrane hydration has involved limited water contents. James et al. recorded phase images over a 1 μm × 1 μm area of dehydrated Nafion as the relative humidity of the imaging environment increased from 9% to 34% RH.[31] The authors observed an increase in the magnitude of phase shifts with increasing relative humidity, yet changes in morphology were not observed in either height or phase images. Our experience indicates that the increase in phase shifts observed by James et al. did not result from changes in properties associated with Nafion, but rather from changes in tip–sample forces associated either with an increase in the thickness of water adsorbed on the membrane's surface (expected for any material exposed to increasing relative

dx.doi.org/10.1021/ma302399e | *Macromolecules* 2013, 46, 2267–2274

humidity) or with inadvertent changes in the cantilever's free space amplitude, which can occur over the course of prolonged imaging due to tip−sample interactions (Figure S1). Furthermore, AFM studies of hydrated PEMs have been limited by imaging membranes or solution cast films that were first hydrated by boiling or soaking in water but then imaged at ambient conditions.[32−34] We find the distinct morphology of hydrated membranes is lost when imaged at ambient conditions instead of at high relative humidity. Current imaging of Nafion has also been explored as a function of relative humidity (30%−84% RH being the widest range investigated).[35−38] These studies have focused on the electrochemical activity at the membrane surface rather than morphology. As such, a distinguishing feature of the work presented here is the wide range of conditions under which Nafion membranes were imaged—from 3% to 95% RH. To our knowledge, there exists no previous scanned probe investigation that explores the surface morphology of Nafion over this span of relative humidities. Knowing what surface morphology facilitates high proton conductivity in Nafion at hydrated conditions will provide a context for developing next-generation polymer electrolytes that maintain high conductivities at conditions necessary to maximize fuel cell heat management (120 °C) and catalyst durability (25% RH).[39] While scanned probe microscopy has been used to describe the nature of proton conducting domains in 3-D,[40] it is used here exclusively to probe the surface of Nafion membranes, which complements the bulk averaged properties typically gleaned from scattering measurements, with exceptions coming from grazing-incidence SAXS[26] and neutron reflectivity experiments.[41] Our observations agree with aspects of models based on scattering measurements yet also reveal morphological features unique to Nafion's surface, highlighting the simplifications and shortcomings of such models.

RESULTS AND DISCUSSION

Nafion Morphology at Ambient Conditions. Phase images reveal dramatic differences in the surface morphology of Nafion 212 membranes at dehydrated, ambient, and hydrated conditions (Figure 1). All images of Nafion were acquired on membranes that were first fully hydrated by boiling in acid and water and then equilibrated at 3%, 49%, and 95% RH. At ambient conditions (49% RH), hydrophilic sulfonic acid side groups (dark contrast) phase separate from Nafion's hydrophobic fluorocarbon backbone (bright contrast), producing a morphology that resembles the rind of a cantaloupe (Figure 1H and Figure S2). The arrangement of hydrophilic and hydrophobic surface domains at ambient conditions agrees with the inverted micelle geometry proposed in the parallel pore model of Nafion.[30] At ambient conditions, hydrophilic domains cover 19% of the surface and have an average size of 94 nm^2 and an occurrence of 2.0 domains per 1000 nm^2. Fitting to a circular geometry yields an average diameter of 11 ± 4 nm for these domains, which agrees with previous AFM studies of Nafion.[22] Hydrophilic and hydrophobic features 5 nm in diameter are clearly resolved, indicating the 11 nm average diameter of hydrophilic domains is not resolution limited. Furthermore, these domain sizes agree with electron microscopy of Nafion stained with solid metal particles,[42,43] but are ∼9 nm larger than that measured with scattering techniques (e.g., 2.4 nm at ∼80% RH in the parallel pore model).[30,44] The latter is an important finding, indicating the arrangement of sulfonic acid groups is much different at the surface of Nafion than in the bulk. Greater-than-bulk sizes of hydrophilic domains indicate a clustering of sulfonic acid domains that are oriented toward the surface, and larger-than-bulk distances between hydrophilic domains correspond to regions where side chains are oriented away from the surface and buried beneath the fluorocarbon backbone.

The rind morphology observed at ambient conditions also closely resembles the bicontinuous network predicted statistically and thermodynamically by Elliot et al.[28] Our analysis of 2-D maximum entropy reconstructions of Nafion shows ion-rich domains in ref 28 cover the same area (20%), yet occur at twice the frequency (3.9 domains per 1000 nm^2) and are approximately half the size (52 nm^2) of ion-rich domains observed in phase images. Side-by-side comparison reveals the 2-D reconstructions do not account for adjoined ion-rich domains as observed at the surface of membranes in phase images, explaining differences between the two techniques in the occurrence and size of such domains (Figure S2). Notably, the morphology predicted in 2-D reconstructions more closely resembles that observed with scanned probe microscopy at ambient conditions than at hydrated conditions, despite reconstructions being based on scattering measurements of membranes at water contents of λ = 14−16 mol H_2O/mol SO_3^-. In our work, similar domain size, shape, occurrence, and coverage were observed for membranes equilibrated at relative humidities ranging from 30% to 75% RH, in agreement with Zawodzinski et al., who reported that Nafion's water content only increased from λ = 2 at 15% RH to λ = 4 at 60% RH.[45] Morphological changes may accompany this small increase in water content; however, such changes were not large enough to be detected with AFM. Finally, at the 250 nm × 250 nm scan size in Figure 1, images of Nafion 117 membranes—prepared by melt extrusion—show surface morphology indistinguishable from Nafion 212, which are dispersion cast.

As phase images can be influenced by more than just the composition of a material, it is important to clarify assignment of contrast in these images. First, interpretation of phase shifts depends on whether tip−sample interactions are attractive (>90°) or repulsive (<90°); it is possible for both types of interactions to exist simultaneously (so-called bistable imaging) yet such conditions do not yield meaningful phase images.[21] As tip−sample power dissipation is related to the sine of the phase angle, contrast is interpreted in terms of power dissipation wherein larger dissipations are associated with phase shifts closer to 90° in both regimes.[18,19] Important to note is that long-range attractive forces dominate tip−sample interactions over a smaller window of operating conditions (i.e., cantilever drive amplitude and the ratio between the set point amplitude and free space amplitude) than repulsive interactions. As tip−sample forces are minimized in attractive mode images, it is often desired to image in this regime. Other than using small oscillation amplitudes (<10 nm) and high Q cantilevers (>200) or Q-control,[46] we have found that the attractive regime is more easily accessed by acquiring phase images while tracking the topography of a sample in a second pass of the sample at a lift height ∼5 nm above the surface (Figure S3). Second, scanned probe studies of Nafion have shown the importance of considering topographic contributions to tip−sample power dissipation in phase images; such crosstalk can exist under both attractive and repulsive regimes, obscuring contrast associated with the mechanical properties of a material.[22] Topography did not influence phase contrast in images taken at dehydrated and ambient conditions, while it did at hydrated conditions

dx.doi.org/10.1021/ma302399e | Macromolecules 2013, 46, 2267−2274

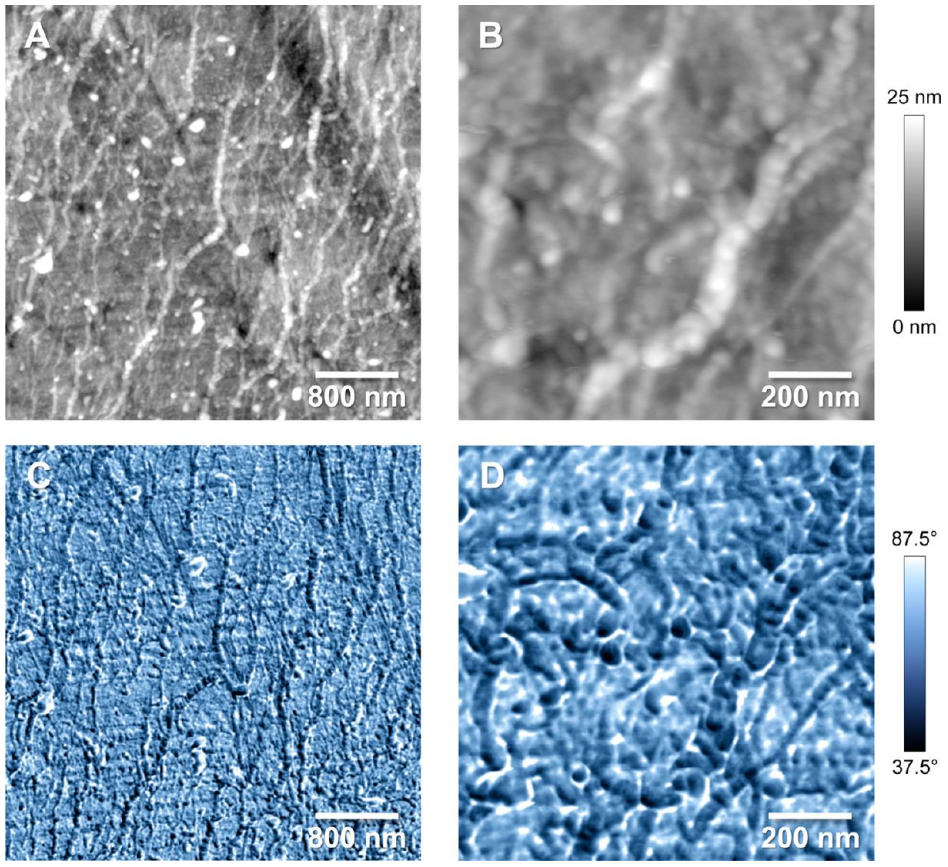

Figure 2. (A, B) Topography and (C, D) phase images of hydrated Nafion 212 imaged at 95% RH and at 4 μm × 4 and 1 μm × 1 μm scan sizes. Elongated, segmented water-swollen domains are visible in both topography and phase images.

(expectedly), necessitating use of conductive probe AFM (cp-AFM) for a full interpretation of the latter (as shown below). Thus, excluding influences of topography, phase images provide insight into tip−sample interactions associated with material composition; in the case of PEMs, this has allowed mapping of hydrophilic and hydrophobic surface domains, where the former are associated with larger tip−sample power dissipations.

Nafion Morphology at Dehydrated Conditions. Images of dehydrated Nafion membranes were acquired at 3% RH after drying hydrated membranes and reveal highly isolated features (bright contrast, Figure 1G); under these conditions, there are less than 2 mol H_2O/mol SO_3^-.[45] Images of dehydrated membranes were taken under net repulsive tip−sample interactions. In this regime, bright regions (phase shifts closer to 90°) correspond to larger tip−sample power dissipation, which we assign as hydrophilic surface domains.[21] Interestingly, these domains have an average size (120 nm^2) similar to those in membranes equilibrated at ambient conditions yet cover nearly 4 times less the area (5.2%) and occur nearly 6 times less frequently (0.35 domains per 1000 nm^2), which is an important finding, suggesting inhomogeneous retention of water among sulfonic acid groups. This agrees with He et al., who observed isolated features with high conductivity in cp-AFM images of Nafion at 30% RH;[38] owing to the higher relative humidity (i.e., 30% RH vs 3% RH), the isolated features were much larger (~200−700 nm in diameter) than those observed in our work (12 ± 5 nm average diameter). The isolated hydrophilic features observed here, however, are 10 times larger than the 1.3−1.5 nm ion clusters determined from bulk scattering experiments of dehydrated Nafion.[30,47] As at ambient conditions, the size of hydrophilic domains was not resolution limited at dehydrated conditions. It is important to note that our data does not preclude the simultaneous existence of 1.3−1.5 nm ion domains at the surface of Nafion; in fact, it is expected that domains with such low water contents would not give rise to measurable phase shifts. Thus, the relatively large (12 ± 5 nm) hydrophilic surface features observed at low water contents points to stark inhomogeneities in the dehydration of clustered proton conducting domains, again highlighting differences between bulk and surface properties of Nafion. Unlike ambient conditions, where attractive mode phase imaging resolves PEM morphology better than repulsive mode due to less interaction with water adsorbed on the membrane's surface,[22] phase contrast is highly resolved (<10 nm) in images of dehydrated membranes under repulsive tip−sample interactions. The lack of water at the surface of dehydrated membranes minimizes long-range attractive forces, making repulsive mode imaging more suited for dehydrated membranes. Attempts to image dehydrated membranes in the attractive regime yielded phase contrast related only to changes in topography, whereas topography did not contribute to phase contrast in repulsive mode images at these conditions (Figure S4).

Nafion Morphology at Hydrated Conditions. Images of hydrated Nafion were taken at 95% RH and reveal features much larger than at lower membrane water contents (Figure 1I). The high density of hydrophilic surface domains at ambient relative humidities is absent at hydrated conditions, suggesting domains coalesce with hydration.[48,49] Larger scans of hydrated

dx.doi.org/10.1021/ma302399e | *Macromolecules* 2013, 46, 2267−2274

Nafion show that the features in Figure 1I comprise segments of elongated, wormlike features that tortuously extend several micrometers over the membrane's surface (Figure 2), in agreement with the ribbon and fibril structures proposed from scattering measurements.[23−26,30] We have observed such elongated features stretch up to 40 μm in length, confirming predictions of large features made by Kim et al. based on ultrasmall-angle neutron scattering.[25] An important feature of the wormlike superstructures in Figures 1I and 2 is that they consist of smaller nodal segments 25−45 nm in diameter. Dynamic light scattering measurements reveal individual Nafion polymer chains have hydrodynamic radii <100 nm,[50] indicating the nodes observed here correspond to individual polymer chains. Remarkably, the elongated features are much wider than they are tall—on average, 15 times wider than they are thick, with widths ranging from 25 to 150 nm (one to several nodes) and heights ranging from 1.5 to 9 nm. Larger, isolated circular features in this image correspond to water droplets on the surface of the membrane; more droplets were observed the sooner hydrated Nafion was imaged after transferring from water. Some of the larger elongated height features persisted several days after storing the hydrated membrane at ambient conditions and to a lesser extent, after dehydrating the membrane, in agreement with the long equilibration times associated with Nafion.[25,51,52] The wormlike features seen in the hydrated membrane also resemble nanofibers of Nafion (reported at 30−50 nm in diameter) formed upon hydration of the catalyst layer in membrane electrode assemblies.[53] Nanofibers of Nafion 400 nm in diameter produced by electrospinning show proton conductivities as high as 1.5 S/cm,[54] suggesting the wormlike features enable efficient proton transport in hydrated membranes.

Macroscopically, we found that the area of hydrated Nafion membranes shrank by 20% after 6 h at ambient conditions. Nearly 60% of this decrease in area occurred within 15 min of removing Nafion from storage in water, making it important to quickly transfer the sample to a humidified environment. Compared to the fully hydrated membrane, imaging at 95% RH in a sealed environment for 5 h resulted in only a 4% decrease in the membrane's area, indicating little change in water content while imaging. These measurements underscore the importance of imaging hydrated membranes under humidified conditions to preserve a membrane's water content.

While proton conducting domains appear perpendicular to the surface in Nafion at dehydrated and ambient conditions, water-swollen domains extend parallel to the surface in hydrated membranes. Unlike ^{2}H NMR experiments that suggest domains align parallel to the surface only in extruded Nafion membranes,[55] we observed in-plane alignment of elongated domains at the surface of both extruded (Nafion 117) and dispersion cast (Nafion 212) membranes. The in-plane alignment of these domains in Nafion 212 agrees with GISAXS of spin-cast Nafion films.[26] Notably, fewer bends appear in the elongated features in extruded membranes, in agreement with Kim et al.[25] That we observe a domain orientation different from that measured with bulk ^{2}H NMR experiments again indicates critical differences in PEM morphology at the surface of a membrane compared to the bulk.

Hydrated Nafion was imaged under net repulsive interactions, as strong tip−sample interactions from adsorbed water caused frequent jumps to contact by the tip, which prevented stable imaging in the attractive regime at high humidities. Such jumps to contact correspond to hopping between the attractive (noncontact) and repulsive (intermittent contact) regimes, resulting in undesired bistable imaging.[21] While phase contrast showed no relation to topography or changes in topography in the dehydrated and ambient cases, it is correlated with topography and changes in topography in the hydrated case, which is expected given the large topographic features in the hydrated membrane (Figure S5). As evident in Figures 1 and 2, the phase image of the hydrated membrane provides a more highly resolved image of membrane's topography.

Because phase contrast in hydrated Nafion membranes is related to topography and changes in topography, we cannot use these images to determine whether the wormlike features consist of a fluorocarbon backbone surrounding sulfonic acid groups (inverted micelle) or vice versa (micelle). Instead, conductive probe AFM was used to determine whether the fibrillar-like features exhibit conductive or insulating behavior, which would point to a micelle or inverted micelle geometry, respectively. Current images of acid-hydrated Nafion 117 reveal a bimodal distribution with low currents measured over the wormlike features (Figure 3B). An identical, low current response was observed over the entire surface of hydrated Nafion in the absence of a sample bias (Figure 3C), indicating an insulating nature of the raised features and providing evidence that the elongated domains consist of a fluorocarbon shell, in agreement with pulsed field gradient spin-echo NMR[56] and contact angle measurements showing the surface of Nafion remains hydrophobic up to 97% RH.[26] Regions of positive current exist between the elongated features, and under positive sample bias, result from oxygen reduction at the interface of proton-rich regions and the Pt-coated AFM tip and concurrent water oxidation at the carbon electrode opposite the tip.[57] This supports the model of Rubatat et al. that water in Nafion membranes is not limited to spherical cavities but exists between fibrillar objects.[23] Because hydrated membranes were imaged at 95% RH, the fluorocarbon exterior of elongated features observed here does not preclude a micelle arrangement of ionic groups expected in Nafion exposed to liquid water[24,26,58] but does indicate an inversion in structure must occur beyond 95% RH. As with phase images, interpretation of current images involves consideration of factors that can affect the measured current other than a material's electrical and electrochemical properties, namely variations in topography and tip−sample contact area. Increased current is commonly observed in cp-AFM as the probe climbs tall topographic features due to greater tip−sample contact areas. Importantly, such artifacts were not present in the current image in Figure 3, evident in the observation that the current signal was independent of the scan direction. Furthermore, elongated features of one height show the same low current response as elongated features of a different height, indicating the absence of capacitance-related current.

■ CONCLUSIONS

Given that proton transport begins and ends at the surface of PEMs and that interfacial mass transport dictates water sorption in PEMs,[59] we investigated the surface morphology of proton conducting domains, complementing bulk averaged material insights gained from scattering measurements. Atomic force microscopy topography, phase, and current images revealed the surface morphology of Nafion membranes is in many ways distinct from the morphology of the rest of the membrane. We observed that Nafion's surface morphology

dx.doi.org/10.1021/ma302399e | Macromolecules 2013, 46, 2267−2274

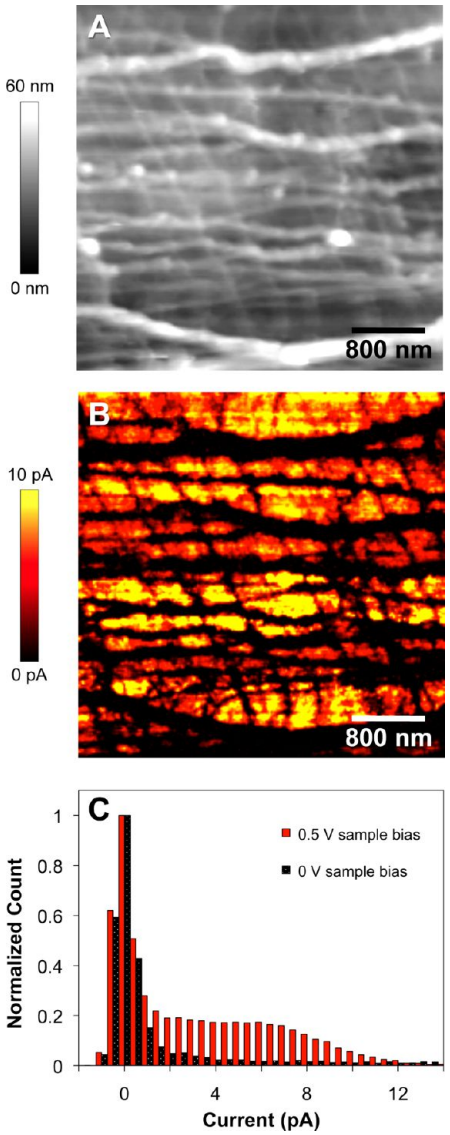

Figure 3. (A) Topography and (B) current images (4 μm × 4 μm) of acid-hydrated Nafion 117 at 0.5 V sample bias. (C) Current distributions of hydrated Nafion imaged at 0.5 V sample bias (red) and 0 V sample bias (dotted black).

evolves from a low density of isolated hydrophilic domains at dehydrated conditions (3% RH) to a network of elongated, yet segmented, wormlike domains that span several micrometers at hydrated conditions (95% RH). Properties unique to Nafion's surface include inhomogeneous dehydration of hydrophilic domains; greater coalescence of sulfonic acid groups and thus larger hydrophilic domain sizes at ambient conditions; and a much larger span of elongated domains at hydrated conditions than previously observed with scattering measurements.[23,24] These observations provide morphological evidence for both the facile and languid conduction of protons observed in Nafion at hydrated and dehydrated conditions, respectively. The sharp differences in surface morphology at different membrane water contents motivates questions regarding how the nanoscale electrochemical activity[35,38,57,60,61] and top to bottom connectivity[40,62−64] of individual proton conducting domains varies with hydration. Interesting questions also remain regarding the dependence of morphology on fuel cell operating temperature,[65] the time scales associated with hydration-induced changes in surface morphology,[51,66] and the extent of morphological memory while cycling through low and high membrane water contents. Such queries can be resolved with techniques such as scanned probe microscopy that allow *in situ* investigation of material properties.

EXPERIMENTAL SECTION

All images were acquired with a MFP-3D atomic force microscope (Asylum Research). Owing to the importance of a membrane's thermal history on its water uptake,[51] images in Figures 1 and 2 were taken on Nafion 212 membranes (Fuel Cell Store, Inc.) initially hydrated by boiling in 0.5 M H_2SO_4 and DI water for 2 h each. Membranes were then stored in DI water at room temperature before dehydrating, equilibrating at ambient conditions, or imaging directly in the hydrated state. Nafion was dehydrated at 105 °C in a vacuum oven for 3.5 days and immediately imaged under dry N_2 (3% RH) in a sealed gas flow cell (Asylum Research). Additional dehydration of membranes resulted in the formation of nodal topographic features (Figure S6). Excess surface water was shaken off hydrated membranes before imaging immediately at 95% RH (obtained by bubbling N_2 through water at room temperature) in a sealed environment. Images in Figure 3 were taken of Nafion 117 (Fuel Cell Store, Inc.) only boiled in 0.5 M H_2SO_4 and dried at ambient conditions for 24 h. An adhesive carbon tab (Ted Pella, Inc.) was used to make electrical contact to the underside of the membrane (without hot pressing) and to hold the membrane in place. A +0.5 V bias (relative to ground and the AFM tip) was applied to the carbon electrode during cp-AFM measurements; nonzero current measured at 0 V bias—common in cp-AFM measurements due to instrument offset—was accounted for with a 5 pA current offset. For the pA currents measured in this work, generation of water at the tip during cp-AFM measurements (less than 1×10^{-19} mol H_2O/point for images taken at 0.004 s/point) did not affect current imaging. For membranes boiled in acid and water and then equilibrated at different relative humidities, we observed no difference between the morphology of the air and substrate side of dispersion-cast Nafion 212 membranes at the 250 nm × 250 nm length scale. At large length scales (i.e., 20 μm × 20 μm scan size), slight, irregularly shaped topographic depressions (~5 nm deep and ≤1 μm^2 in size) were seen in the substrate side of the membrane (side with thick backing sheet) both before and after hydration. Phase and corresponding height images were taken in ac mode (amplitude modulation) with silicon probes (NSC15, MikroMasch). Current and corresponding height images were acquired in contact mode with Pt−Ir-coated probes (EFM, Nanoworld). In all images, analysis of proton conducting domains included only those larger than 20 nm^2 as to account for the size of the AFM tip. Masks used to quantify domain size, occurrence, and surface area in Figure 1 were determined using the iterative selection method[67] and are shown in the Supporting Information (Figure S5).

ASSOCIATED CONTENT

Supporting Information

Phase contrast of Nafion as a function of amplitude set point ratio; the rindlike morphology of Nafion at ambient conditions; use of two-pass imaging to more easily access attractive tip−sample interactions; images of dehydrated Nafion acquired under net attractive tip−sample interactions; masks of phase contrast overlaid on images of topography and changes in topography of Nafion at dehydrated, ambient, and hydrated conditions; and topography of Nafion after prolonged dehyration. This material is available free of charge via the Internet at http://pubs.acs.org.

AUTHOR INFORMATION

Corresponding Author

*E-mail: buratto@chem.ucsb.edu.

Present Address
[†]Department of Chemistry and Chemical Biology, Cornell University, Ithaca, NY 14853-1301.

Notes
The authors declare no competing financial interest.

■ ACKNOWLEDGMENTS

The authors thank David A. Bussian for useful discussions at the onset of this work. This work was supported by the MURI and DURIP programs of the U.S. Army Research Laboratory and U.S. Army Research Office under grants DAAD 19-03-1-0121 and W911NF-09-1-0280. J.R.O. acknowledges the UCSB Graduate Student Science and Engineering Research Grant. N.J.E. acknowledges the NSF Graduate Fellowship Research Program. This work utilized facilities in UCSB's Materials Research Laboratory, supported by the MRSEC Program of the National Science Foundation under grant DMR05-20415.

■ REFERENCES

(1) Schuster, M. F. H.; Meyer, W. H. *Annu. Rev. Mater. Sci.* **2003**, *33*, 233−261.
(2) Xiao, L.; Zhang, H.; Scanlon, E.; Ramanathan, L. S.; Choe, E.-W.; Rogers, D.; Apple, T.; Benicewicz, B. C. *Chem. Mater.* **2005**, *17*, 5328−5333.
(3) Kim, S. Y.; Kim, S.; Park, M. J. *Nat. Commun.* **2010**, *1*, 88.
(4) Kannan, R.; Aher, P. P.; Palaniselvam, T.; Kurungot, S.; Kharul, U. K.; Pillai, V. K. *J. Phys. Chem. Lett.* **2010**, *1*, 2109−2113.
(5) Zawodzinski, T. A.; Neeman, M.; Sillerud, L. O.; Gottesfeld, S. *J. Phys. Chem.* **1991**, *95*, 6040−6044.
(6) Sone, Y.; Ekdunge, P.; Simonsson, D. *J. Electrochem. Soc.* **1996**, *143*, 1254−1259.
(7) Kreuer, K.-D.; Paddison, S. J.; Spohr, E.; Schuster, M. *Chem. Rev.* **2004**, *104*, 4637−4678.
(8) Devanathan, R.; Venkatnathan, A.; Dupuis, M. *J. Phys. Chem. B* **2007**, *111*, 8069−8079.
(9) Feng, S.; Voth, G. A. *J. Phys. Chem. B* **2011**, *115*, 5903−5912.
(10) Agmon, N. *Chem. Phys. Lett.* **1995**, *244*, 456−462.
(11) Kreuer, K.-D.; Rabenau, A.; Weppner, W. *Angew. Chem., Int. Ed.* **1982**, *21*, 208−209.
(12) Ding, J.; Chuy, C.; Holdcroft, S. *Macromolecules* **2002**, *35*, 1348−1355.
(13) Elabd, Y. A.; Napadensky, E.; Walker, C. W.; Winey, K. I. *Macromolecules* **2006**, *39*, 399−407.
(14) Elabd, Y. A.; Hickner, M. A. *Macromolecules* **2010**, *44*, 1−11.
(15) Park, M. J.; Downing, K. H.; Jackson, A.; Gomez, E. D.; Minor, A. M.; Cookson, D.; Weber, A. Z.; Balsara, N. P. *Nano Lett.* **2007**, *7*, 3547−3552.
(16) Tsang, E. M. W.; Zhang, Z.; Shi, Z.; Soboleva, T.; Holdcroft, S. *J. Am. Chem. Soc.* **2007**, *129*, 15106−15107.
(17) Wilson, M. S.; Gottesfeld, S. *J. Appl. Electrochem.* **1992**, *22*, 1−7.
(18) Tamayo, J.; Garcia, R. *Appl. Phys. Lett.* **1998**, *73*, 2926−2928.
(19) Cleveland, J. P.; Anczykowski, B.; Schmid, A. E.; Elings, V. B. *Appl. Phys. Lett.* **1998**, *72*, 2613−2615.
(20) McLean, R. S.; Doyle, M.; Sauer, B. B. *Macromolecules* **2000**, *33*, 6541−6550.
(21) James, P. J.; Antognozzi, M.; Tamayo, J.; McMaster, T. J.; Newton, J. M.; Miles, M. J. *Langmuir* **2001**, *17*, 349−360.
(22) O'Dea, J. R.; Buratto, S. K. *J. Phys. Chem. B* **2011**, *115*, 1014−1020.
(23) Rubatat, L.; Rollet, A. L.; Gebel, G.; Diat, O. *Macromolecules* **2002**, *35*, 4050−4055.
(24) Rubatat, L.; Gebel, G.; Diat, O. *Macromolecules* **2004**, *37*, 7772−7783.
(25) Kim, M.-H.; Glinka, C. J.; Grot, S. A.; Grot, W. G. *Macromolecules* **2006**, *39*, 4775−4787.
(26) Bass, M.; Berman, A.; Singh, A.; Konovalov, O.; Freger, V. *J. Phys. Chem. B* **2010**, *114*, 3784−3790.
(27) Schmidt-Rohr, K.; Chen, Q. *Nat. Mater.* **2008**, *7*, 75−83.
(28) Elliott, J. A.; Wu, D.; Paddison, S. J.; Moore, R. B. *Soft Matter* **2011**, *7*, 6820−6827.
(29) Mauritz, K. A.; Moore, R. B. *Chem. Rev.* **2004**, *104*, 4535−4585.
(30) Kong, X.; Schmidt-Rohr, K. *Polymer* **2011**, *52*, 1971−1974.
(31) James, P. J.; McMaster, T. J.; Newton, J. M.; Miles, M. J. *Polymer* **2000**, *41*, 4223−4231.
(32) Chomakovahaefke, M.; Nyffengger, R.; Schmidt, E. *Appl. Phys. A: Mater. Sci. Process.* **1994**, *59*, 151−153.
(33) Lehmani, A.; Durand-Vidal, S.; Turq, P. *J. Appl. Polym. Sci.* **1998**, *68*, 503−508.
(34) Affoune, A. M.; Yamada, A.; Umeda, M. *J. Power Sources* **2005**, *148*, 9−17.
(35) O'Hayre, R.; Lee, M.; Prinz, F. B. *J. Appl. Phys.* **2004**, *95*, 8382−8392.
(36) Aleksandrova, E.; Hiesgen, R.; Eberhard, D.; Friedrich, K. A.; Kaz, T.; Roduner, E. *ChemPhysChem* **2007**, *8*, 519−522.
(37) Takimoto, N.; Wu, L.; Ohira, A.; Takeoka, Y.; Rikukawa, M. *Polymer* **2009**, *50*, 534−540.
(38) He, Q.; Kusoglu, A.; Lucas, I. T.; Clark, K.; Weber, A. Z.; Kostecki, R. *J. Phys. Chem. B* **2011**, *115*, 11650−11657.
(39) Mathias, M. F.; Makharia, R.; Gasteiger, H. A.; Conley, J. J.; Fuller, T. J.; Gittleman, C. J.; Kocha, S. S.; Miller, D. P.; Mittelsteadt, C. K.; Xie, T.; Yan, S. G.; Yu, P. T. *Electrochem. Soc. Interface* **2005**, *14*, 24−35.
(40) Gargas, D. J.; Bussian, D. A.; Buratto, S. K. *Nano Lett.* **2005**, *5*, 2184−2187.
(41) Dura, J. A.; Murthi, V. S.; Hartman, M.; Satija, S. K.; Majkrzak, C. F. *Macromolecules* **2009**, *42*, 4769−4774.
(42) Rollins, H. W.; Lin, F.; Johnson, J.; Ma, J.-J.; Liu, J.-T.; Tu, M.-H.; DesMarteau, D. D.; Sun, Y.-P. *Langmuir* **2000**, *16*, 8031−8036.
(43) Sun, Y.; Atorngitjawat, P.; Lin, Y.; Liu, P.; Pathak, P.; Bandara, J.; Elgin, D.; Zhang, M. *J. Membr. Sci.* **2004**, *245*, 211−217.
(44) Zawodzinski, T. A.; Springer, T. E.; Uribe, F.; Gottesfeld, S. *Solid State Ionics* **1993**, *60*, 199−211.
(45) Zawodzinski, T. A.; Springer, T. E.; Davey, J.; Jestel, R.; Lopez, C.; Valerio, J.; Gottesfeld, S. *J. Electrochem. Soc.* **1993**, *140*, 1981−1985.
(46) Rodriguez, T. R.; Garcia, R. *Appl. Phys. Lett.* **2003**, *82*, 4821−4823.
(47) Gebel, G. *Polymer* **2000**, *41*, 5829−5838.
(48) Gierke, T. D.; Munn, G. E.; Wilson, F. C. *J. Polym. Sci., Polym. Phys.* **1981**, *19*, 1687−1704.
(49) Malek, K. *J. Chem. Phys.* **2008**, *129*, 204702.
(50) Chen, H.; Snyder, J. D.; Elabd, Y. A. *Macromolecules* **2008**, *41*, 128−135.
(51) Onishi, L. M.; Prausnitz, J. M.; Newman, J. *J. Phys. Chem. B* **2007**, *111*, 10166−10173.
(52) Satterfield, M. B.; Benziger, J. B. *J. Polym. Sci., Part B: Polym. Phys.* **2009**, *47*, 11−24.
(53) Snyder, J. D.; Elabd, Y. A. *J. Power Sources* **2009**, *186*, 385−392.
(54) Dong, B.; Gwee, L.; Salas-de la Cruz, D.; Winey, K. I.; Elabd, Y. A. *Nano Lett.* **2010**, *10*, 3785−3790.
(55) Li, J.; Wilmsmeyer, K. G.; Madsen, L. A. *Macromolecules* **2008**, *41*, 4555−4557.
(56) Zhao, Q.; Majsztrik, P.; Benziger, J. *J. Phys. Chem. B* **2011**, *115*, 2717−2727.
(57) Hiesgen, R.; Aleksandrova, E.; Meichsner, G.; Wehl, I.; Roduner, E.; Friedrich, K. A. *Electrochim. Acta* **2009**, *55*, 423−429.
(58) Goswami, S.; Klaus, S.; Benziger, J. *Langmuir* **2008**, *24*, 8627−8633.
(59) Satterfield, M. B.; Benziger, J. B. *J. Phys. Chem. B* **2008**, *112*, 3693−3704.
(60) Bussian, D. A.; O'Dea, J. R.; Metiu, H.; Buratto, S. K. *Nano Lett.* **2007**, *7*, 227−232.
(61) Xie, X.; Kwon, O.; Zhu, D. M.; Van Nguyen, T.; Lin, G. Y. *J. Phys. Chem. B* **2007**, *111*, 6134−6140.
(62) Chou, J.; McFarland, E. W.; Metiu, H. *J. Phys. Chem. B* **2005**, *109*, 3252−3256.

(63) Chou, J.; Jayaraman, S.; Ranasinghe, A. D.; McFarland, E. W.; Buratto, S. K.; Metiu, H. *J. Phys. Chem. B* **2006**, *110*, 7119−7121.
(64) Kubo, W.; Yamauchi, K.; Kumagai, K.; Kumagai, M.; Ojima, K.; Yamada, K. *J. Phys. Chem. C* **2010**, *114*, 2370−2374.
(65) Kwon, O.; Wu, S.; Zhu, D.-M. *J. Phys. Chem. B* **2010**, *114*, 14989−14994.
(66) Kusoglu, A.; Modestino, M. A.; Hexemer, A.; Segalman, R. A.; Weber, A. Z. *ACS Macro Lett.* **2012**, *1*, 33−36.
(67) Ridler, T. W.; Calvard, S. *IEEE Trans. Syst., Man Cybern.* **1978**, *8*, 630−632.